Volume 21 | Number 23 | 21 June 2019 | Pages 3527–3646

CrystEngComm

rsc.li/crystengcomm

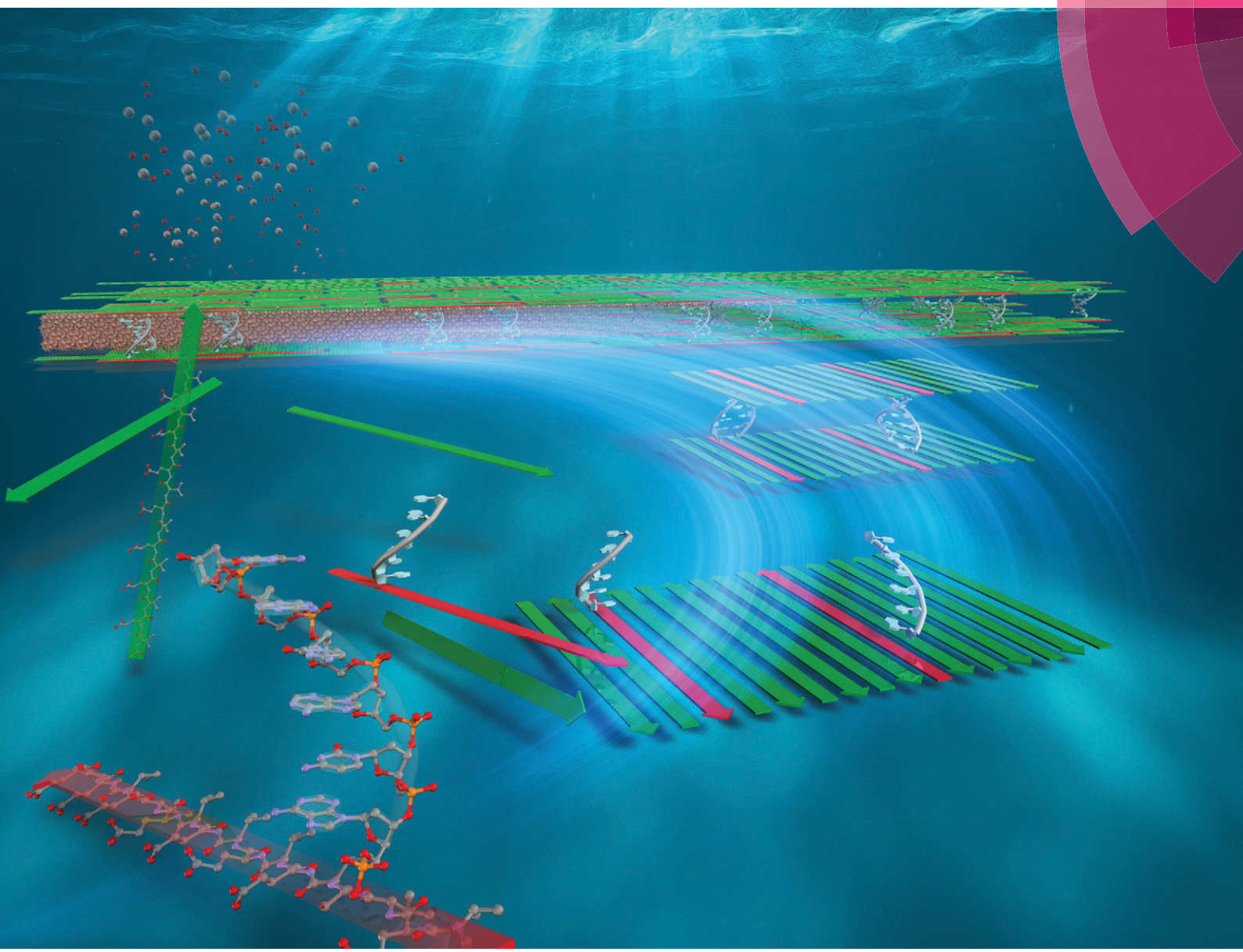

ISSN 1466-8033

ROYAL SOCIETY OF CHEMISTRY | Celebrating IYPT 2019

PAPER

Kazuki Murai, Masahiro Higuchi *et al.*

Mineralization of magnetic nano-tape in self-organized nanospace composed of nucleopeptides and peptides

CrystEngComm

PAPER

View Article Online
View Journal | View Issue

Cite this: *CrystEngComm*, 2019, **21**, 3557

Mineralization of magnetic nano-tape in self-organized nanospace composed of nucleopeptides and peptides†

Kazuki Murai, *[a] Kaede Inagaki,[b] Chisato Hiraoka,[b] Sayaka Minoshima,[b] Takatoshi Kinoshita,[c] Kenji Nagata[b] and Masahiro Higuchi*[b]

Received 29th January 2019,
Accepted 24th April 2019

DOI: 10.1039/c9ce00146h

rsc.li/crystengcomm

Self-organization based on specific interactions has been actively studied for the formation of highly ordered and hierarchical structures on the molecular scale. We designed and synthesized a nucleopeptide, Ac-VEVS(g(GC)$_3$)(VE)$_7$-CONH$_2$, having a nucleotide graft-chain in a peptide main-chain, and a spacer peptide acting as a template for ferric oxide mineralization. The synthesized nucleopeptide and spacer peptide mixture formed a self-organized assembly having a nanospace owing to the complementary base pairing between the nucleotide graft-chains of the nucleopeptides and intermolecular hydrogen-bonding between the peptide chains on the substrates. In this study, we report the selective mineralization of magnetite in the nanospace which acted as a reaction field. Mineralized magnetite formed an oriented nano-tape, whose morphology was similar to that of the template nanosheet. This implies that the nanospace in the ordered nanosheet formed by self-organization processes of the nucleopeptide and spacer peptide is extremely useful as a reaction field for the mineralization of structure-controlled magnetite.

Introduction

In recent years, self-organization based on specific interactions between building blocks (peptides and DNA molecules) has been actively studied for the formation of highly ordered and hierarchical structures at the molecular scale. DNA molecules, having the property of rigorous molecular recognition, take a double-helical conformation due to hydrogen bonding between the complementary base pairs (A/T and G/C). DNA nanotechnology has been reported as a strategy for the formation of nanostructures, such as DNA origami[1,2] and DNA tiles.[3,4] On the other hand, peptides take several second-order structures by tuning the primary structure, and the second-order structure can be controlled by external environmental changes. Hence, peptides form many types of assemblies (*e.g.* rods,[5] fibers,[6–8] tapes,[9,10] and micelles[11,12]) based on the second-order structures by self-organization processes using non-covalent interactions, such as hydrogen bonding, coordinate binding, hydrophobic interactions, and electrostatic interactions. Regular structure-formations by self-organization are attracting attention for development of functional materials in the field of nanotechnology.

Living organisms have several biominerals (*e.g.*, bones, seashells, and magnetosomes) with hierarchically organized structures at the nanoscale. Biominerals are observed in many organisms, such as animals, plants, and bacteria.[13–17] These biominerals are formed under mild conditions at ordinary temperatures and pressures by unique self-organization processes of organic and inorganic matter, known as biomineralization. Biominerals exhibit numerous functions owing to their ordered and hierarchical structures. Therefore, the development of functional organic–inorganic hybrid nanomaterials utilizing bioinspired fabrication processes has been actively studied. In previous studies, peptides and proteins have been used as organic templates for mineralization.[18–21] In particular, we have focused on peptides as a powerful tool to understand the mechanisms of biomineralization. Because peptides form ordered assembly structures based on their second-order structures, we can control the arrangement of functional groups of amino-acid side-chains in the structure from angstrom- to nano-scales. In fact, we have reported that the morphology and crystal structure of mineralized inorganic matter (*e.g.*, silica, calcium carbonate, and calcium phosphate) were regulated by the special arrangements of the

[a] *Department of Chemistry and Materials, Faculty of Textile Science and Technology, Shinshu University, 3-15-1 Tokida, Ueda, Nagano 386-8567, Japan. E-mail: murai_kazuki@shinshu-u.ac.jp*
[b] *Department of Life Science and Applied Chemistry, Graduate School of Engineering, Nagoya Institute of Technology, Gokiso-cho, Showa-ku, Nagoya 466-8555, Japan. E-mail: higuchi.masahiro@nitech.ac.jp*
[c] *Nagoya Institute of Technology, Gokiso-cho, Showa-ku, Nagoya 466-8555, Japan*

† Electronic supplementary information (ESI) available: Schemes of the growth mechanism and synthesis strategy of the nucleopeptide, TEM images of the nucleopeptide/spacer peptide aggregates obtained in the aqueous solution at pH 6.5, UV-vis spectra and ^{1}HNMR spectra of the nucleopeptide. See DOI: 10.1039/c9ce00146h

functional groups of amino-acid side-chains and morphologies of the designed peptide templates.[8,19,20,22,23]

Magnetite as a bio-inorganic matter is a functional material having magnetic properties, and has been widely applied to engineering and medical fields. Therefore, mineralization of magnetite with controlled size, morphology, and crystal structure has been investigated.[24–27] In this study, we report the selective mineralization of magnetic nano-tape in a nanospace formed by self-organization of a nucleopeptide and spacer peptide. We designed and synthesized a nucleopeptide having a nucleotide graft-chain in a peptide main-chain and a spacer peptide having an alternating amphiphilic amino-acid sequence that acted as a template for ferric oxide mineralization. The nucleopeptides and spacer peptides formed self-organized nanosheets owing to rigorous molecular recognition based on the complementary base pairing between the nucleotide graft-chains, and the intermolecular hydrogen-bonding between the peptide chains took a β-sheet conformation. The nanosheets composed of the nucleopeptides and spacer peptides had ordered nanospaces in the interior. We used the nanospace as a ferric oxide mineralization field to fabricate magnetic nano-tape. The concept of the formation of the nanospace and mineralization is shown in Scheme 1.

Experimental

Materials

The synthesis strategy of the nucleopeptide, Ac-VEVS(g(GC)$_3$)(VE)$_7$-CONH$_2$, is shown in Fig. S1.† Firstly, the peptide main-chain, Ac-VEVS(VE)$_7$-CONH$_2$, of the nucleopeptide was synthesized on CLEAR-amide resin (Peptide Inst. Inc.) by 9-fluorenylmethoxycarbonyl (Fmoc) chemistry. After the selective deprotection of the N^{ω}-trityl group of Ser(Trt), the nucleotide graft-chain, 3′-(GC)$_3$-5′, was synthesized from the hydroxyl group of the Ser side-chain on the resin by the phosphoramidite method. Fmoc-amino acids, Fmoc-Val-OH and Fmoc-Glu(OBu^t)-OH (OBu^t; *tert*-butyloxy) were purchased from Peptide Inst. Inc. Fmoc-Ser(Trt)-OH (Trt, N^{ω}-trityl) was purchased from Watanabe Chem. Industries Ltd. Phosphoramidites, 3′-[(2-cyanoethyl)-*N*,*N*-diisopropyl]-phosphoramidite (5′-(DMTr)-*N*-iBu-2′-dG) and 3′-[(2-cyanoethyl)-(*N*,*N*-diisopropyl)]-phosphoramidite (5′-(DMTr)-*N*-Bz-2′-dC), were purchased from LGC Biosearch Technologies. These abbreviations, DMTr, iBu, Bz, dGe, and dC, mean 4,4′-dimethoxytrityl, isobutyryl, benzoyl, deoxyguanosine, and deoxycytidine, respectively. The detailed procedures are as follows.

Synthesis of the peptide main-chain of the nucleopeptide and spacer peptide

The peptide main-chain, Ac-VEVS(VE)$_7$-CONH$_2$, of the nucleopeptide and the spacer peptide, AC-(VE)$_9$-CONH$_2$, were synthesized by solid-phase peptide synthesis using Fmoc chemistry. The CLEAR-amide resin (500 mg, 0.38 meq g^{-1}) was swollen in 5 mL of dichloromethane (DCM) for 1 d, then rinsed with 5 mL of *N*,*N*-dimethylformamide (DMF) five times. The peptide chains were synthesized on the resin by using Fmoc-amino acids (3 equiv.), 1-hydroxy-7-azabenzotriazole (3 equiv.), and 1,3-diisopropylcarbodiimide (3 equiv.) in DMF for coupling, and 20 vol% piperidine/DMF solution for Fmoc-group removal. To cap the N-terminal amino group of the synthesized peptides on the resin with an acetyl group, the resin

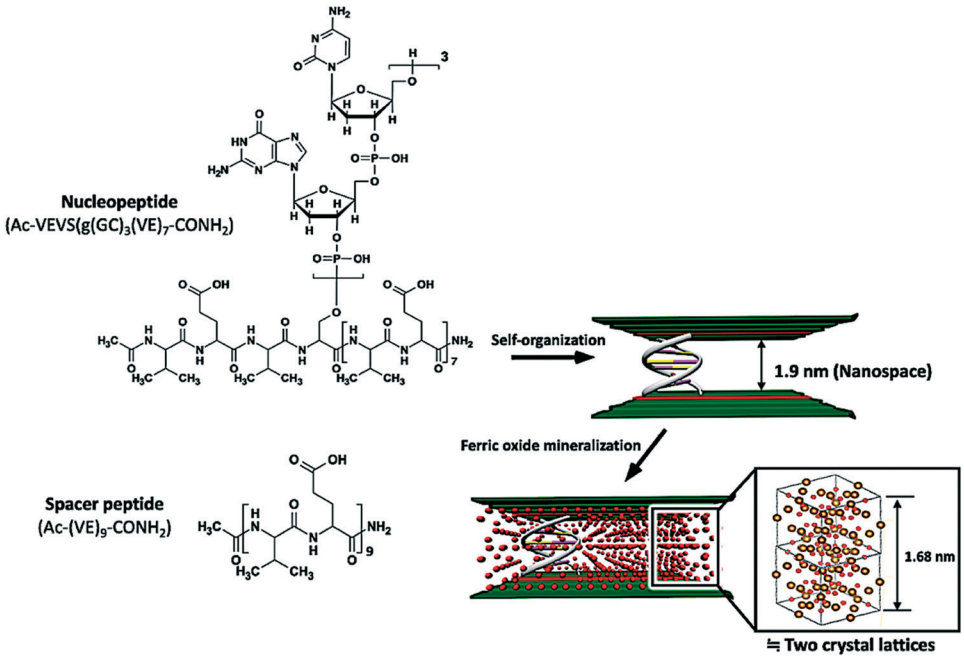

Scheme 1 Schematic picture of formation of the 3D nanostructure composed of the nucleopeptide and spacer peptide by self-organization, and ferric oxide mineralization in the nanospace of the 3D nanostructure.

was stirred in a mixture of acetic anhydride and pyridine (v/v 1/2) for 4 h. The resin was rinsed with DCM to obtain Ac-VE(OBu^t)VS(Trt)(VE(OBu^t))$_7$-CONH-resin and Ac-(VE(OBu^t))$_9$-CONH-resin, respectively. To cleave Ac-(VE)$_9$-CONH$_2$ from the resin and remove the side-chain protecting groups, the Ac-(VE(OBu^t))$_9$-CONH-resin was treated with a 95 vol% trifluoroacetic acid (TFA) aqueous solution. The obtained peptide, Ac-(VE)$_9$-CONH$_2$, was identified using ^{1}H nuclear magnetic resonance (^{1}HNMR, 400 MHz, Bruker AVANCE 500US; Fig. S2†) spectroscopy. The protecting group, Trt, of the Ser residue in the obtained Ac-VE(OBu^t)VS(Trt)(VE(OBu^t))$_7$-CONH-resin was selectively removed using a DCM solution containing 1 vol% TFA and 5 vol% triisopropylsilane. After the selective removal of the Trt group, a part of the Ac-VE(OBu^t)VS(VE(OBu^t))$_7$-CONH-resin was treated with a 95 vol% TFA aqueous solution to obtain Ac-VEVS(VE)$_7$-CONH$_2$. The synthesis of the peptide main-chain, Ac-VEVS(VE)$_7$-CONH$_2$, was confirmed by ^{1}HNMR spectroscopy (Fig. S3†).

Synthesis of the nucleotide graft-chain of the nucleopeptide

The nucleotide graft-chain, 3′-(GC)$_3$-5′, was synthesized from the hydroxyl group of the Ser side-chain on the Ac-VE(OBu^t)VS(VE(OBu^t))$_7$-CONH-resin using phosphoramidite chemistry. The nucleotide graft-chain was synthesized on the Ac-VE(OBu^t)VS(VE(OBu^t))$_7$-CONH-resin by using phosphoramidites (1.2 mmol) in 2.0 mL of dry acetonitrile (ACN) and tetrazoyl (0.45 M) in 2.0 mL of dry ACN for coupling, and 5 mL of oxidizing agent (0.1 M/I$_2$, tetrahydrofuran : pyridine : H$_2$O (v : v : v = 70 : 20 : 2)) for oxidation of the phosphodiester bond and a 3 vol% trichloroacetic acid (TCA)/DCM solution for DMTr group removal. To remove OBu^t groups of the Glu residues in the peptide main-chain and cleave the nucleopeptide molecule from the resin, the Ac-VE(OBu^t)VS(g(G(iBu)C(Bz))$_3$)(VE(OBu^t))$_7$-CONH-resin was treated with a 95 vol% TFA aqueous solution. The obtained Ac-VEVS(g(G(iBu)C(Bz))$_3$)(VE)$_7$-CONH$_2$ was treated with a 50 vol% NH$_3$/dioxane solution to remove the 2-cyanoethyl, iBu, and Bz protecting groups of the nucleotide graft-chain. The resulting nucleopeptide, Ac-VEVS(g(GC)$_3$)(VE)$_7$-CONH$_2$ was identified by ^{1}HNMR spectroscopy (Fig. S4†).

Immobilization of self-organized nucleotide/spacer peptide assemblies on substrates

The nucleopeptides and spacer peptides were added to H$_2$O, and the pH of each suspension was adjusted to be above pH 10.0 using a 0.1 M NaOH aqueous solution to completely dissolve the nucleopeptides and spacer peptides. We mixed the solutions at 1 : 5 or 1 : 6 molar ratios of the nucleopeptide : spacer peptide. The pH of the mixed solution was readjusted to each pH condition (6.5, 7.0, and 7.5), and the final total concentration of the nucleopeptides and spacer peptides was fixed at 0.1 mM. The mixed solutions were incubated for various periods at room temperature to examine the conformational changes of the peptides and nucleopeptides in the solution.

Immobilizations of the self-organized nucleotide/spacer peptide assemblies on substrates were carried out as follows. A freshly cleaved mica and elastic carbon-coated scanning transmission electron microscope (STEM) grid were immersed into the above prepared mixed solutions at each pH condition for 10 d at 15 °C. After the incubation, the substrates were rinsed with H$_2$O and stored in a desiccator until use.

Ferric oxide mineralization

Ferric oxide mineralization was carried out by immersing the nucleopeptide/spacer peptide nanosheets on the substrates prepared above into an aqueous solution containing 0.05 mM $FeCl_2$ and 0.025 mM $FeCl_3$ for 7 d at 15 °C. We used this molar ratio because magnetite is a compound with a 1 : 2 molar ratio of Fe(II)/Fe(III). After the incubation, the substrates were rinsed with H$_2$O and stored in a desiccator until use.

Microscopic measurements

We observed the morphologies of the nucleopeptide/spacer peptide assemblies before and after mineralization using a STEM (JEM-z2500, JEOL. Ltd.) equipped with an Ultra Scan CCD camera (Orius Camera, Gatan Inc.) in TEM mode. Elemental analysis and mapping of the hybrid nanosheets were performed in an STEM equipped with an energy dispersive X-ray (EDX) spectrometer. The crystal phase of the mineralized ferric oxide in the hybrid nanosheets was examined by selected area electron diffraction (SAED). TEM and STEM observations were performed using unstained samples, at an accelerating voltage of 200 kV.

The magnetic and mechanical properties of the hybrid nanosheet surfaces before and after ferric oxide mineralization were estimated from peak-force tapping quantitative nanomechanical mapping mode (PF-QNM) atomic force microscopy (AFM) observations. The images were collected on a Nanoscope Multimode 8 (Bruker). We used a silicon cantilever whose tip and back sides were coated with Co/Cr (225 μm in length, 20 nm tip radius, and 2.8 N m^{-1} spring constant). A south pole was induced on the tip surface by a magnetizer. We simultaneously acquired a magnetic force mapping that was obtained from adhesion, with modulus and height images. Only the height images were flattened and no further image processing for other images was performed.

Spectroscopic measurements

The second-order structures of the peptide chains in the nucleopeptide and spacer peptide mixed aqueous systems under various conditions were determined by circular dichroism (CD) measurements. CD spectra were recorded on a spectropolarimeter (J-820, JASCO Co., Ltd.) at room temperature under a nitrogen atmosphere. The experiments were performed in a quartz cell with a 1 mm path length over the range of 190–260 nm. Molar ellipticities, $[\theta]_\lambda$, were calculated using the concentration of amino acid residues in the solution.

To investigate the formation of complementary hydrogen bonding between the nucleotide graft-chains, we performed UV-vis measurements of the nucleopeptide and spacer peptide mixed aqueous systems. UV-vis spectra were recorded on a UV-3600 (Shimadzu Co., Ltd) system, in a quartz cell with a 5 mm path length over the range 200–350 nm. The obtained UV-vis spectra were analyzed as the sum of the spectra of the absorption and scattering components. The sum of the calculated components was best fit to the experimental spectra.[20] The obtained absorption spectra showed the molar absorption coefficient, ε_{base}, calculated using the concentration of base residues in the solutions. On the other hand, the scattering components showed the molar absorption coefficient, ε_{scat}, calculated using the total concentration of the nucleopeptides and spacer peptides in the solutions.

Results and discussion

Molecular design of the building blocks to form self-organized nanosheets having a nanospace in the interior

We synthesized the nucleopeptide, Ac-VEVS(g$(GC)_3$)$(VE)_7$-$CONH_2$, composed of the peptide main-chain having an Ac-VEVS$(VE)_7$-$CONH_2$ sequence and the nucleotide graft-chain consisting of a 3′-$(GC)_3$-5′ base sequence, which were designed for the addition of different functions. The peptide main-chain of the nucleopeptide could act as a template for mineralization based on the formation of ordered nanostructures induced by molecular programming. The primary structure of the peptide chain was designed by alternating the amphiphilic sequence containing hydrophilic (Glu) and hydrophobic (Val) amino acids to form a β-sheet conformation. In addition, Glu, having an acidic functional group, would act as the origin of nucleation for the formation of ferric oxide on the template. The nucleotide graft-chain was introduced at the 4th residue Ser side-chain from the N-terminus of the peptide main-chain. The nucleotide graft-chain is exposed on the hydrophilic surface of the nanosheet when the peptide chains take a β-sheet conformation. The nucleotide graft-chain acts as a bridging site between the peptide sheets composed of β-sheet peptides. The repeating (G–C) base sequence easily forms a Z-type double helical structure, whose diameter (1.8 nm) is smaller than the B-type double helical structure.[28] When the peptide main-chains take a β-sheet conformation by intermolecular hydrogen bonding, the distance between β-strands is 0.465 nm.[29] The diameter of the Z-type double helical structure is larger than the distances between β-strands in the β-sheet. Hence, simultaneous formations of a double helical structure and β-sheet conformation would be inhibited in an assembly composed of only nucleopeptides due to steric hindrance. To solve this problem, we mixed the spacer peptide, Ac-$(VE)_9$-$CONH_2$, having basically the same sequence as the main-chain of the nucleopeptide to form the nanosheet. As a result, the nucleopeptides and spacer peptides could form a self-organized nanosheet having a nanospace in the interior. We attempted to use the nanospace as a reaction field for ferric oxide mineralization (Scheme 1). We selected two types of molar ratios of the nucleopeptide and spacer peptide, 1 : 5 and 1 : 6 (Fig. S5a†).

Structural changes of the nucleopeptide and spacer peptide in aqueous solution

Firstly, we investigated the time-dependent conformational changes of the peptide chains in the mixed aqueous system containing the nucleopeptide and spacer peptide using circular dichroism (CD) spectroscopy. The molar ratio of the nucleopeptide and spacer peptide was fixed at 1 : 5. Fig. 1 shows CD spectral changes at each pH condition (pH 6.5; Fig. 1(a), pH 7.0; Fig. 1(b), and pH 7.5; Fig. 1(c)). The CD spectra of the initial states at all the pH conditions show typical random coil patterns having a negative maximum at 198 nm. However, only at the pH 6.5 condition did the spectra change from random coil to β-sheet patterns having a negative maximum at 218 nm after the incubation time. To investigate the dynamics of the conformational changes, the time-dependent changes of molar ellipticity at 218 nm, $[\theta]_{218}$, attributed to the β-sheet conformation, are shown in the bottom row of Fig. 1. At pH 7.0 (Fig. 1(e)) and 7.5 (Fig. 1(f)) conditions, the $[\theta]_{218}$ did not change during the incubation time. On the other hand, at pH 6.5, the negative value of $[\theta]_{218}$ was increased after 5 d of incubation. This implies that the conformational transition of the peptide chains in the mixed system at the pH 6.5 condition had an induction period of 5 d. The peptide chains at pH 6.5 showed a conformational transition from a random coil to a β-sheet within the induction period.

Next, we investigated the conformational changes of the nucleotide graft-chain in the mixed aqueous system using UV-vis spectroscopy. The top row of Fig. S6† shows the UV-vis spectral changes at each pH condition after the incubation period. The spectra were separated into absorption (Fig. S6† middle row) and scattering (Fig. S6† bottom row) components by deconvolution. It is well-known that the base pairing in the nucleotide chains induces a decrease in absorbance around 260 nm. We investigated the molar absorption coefficient, $\varepsilon_{base\ max}$, changes around 260 nm based on the hypochromic effect induced by the formation of the base pair. The top row of Fig. 2 shows the time-dependent changes of the $\varepsilon_{base\ max}$ at the various pH conditions (6.5, 7.0 and 7.5). The $\varepsilon_{base\ max}$ showed the hypochromic effect due to the formation of the base pair between the nucleotides under all pH conditions. Interestingly, these hypochromic effects appeared conspicuously for the early stage of 5 d. Furthermore, we evaluated the turbidity changes of the mixed aqueous system containing the nucleopeptide and spacer peptide with incubation from the molar absorption coefficient, $\varepsilon_{scat\ 300}$, of the scattering components (Fig. 2 bottom row). At pH 7.5, the $\varepsilon_{scat\ 300}$ of the solution did not change (Fig. 2(f)), and the value at pH 7.0 (Fig. 2(e)) slightly increased after the incubation time. On the other hand, at pH 6.5 (Fig. 2(d)) the $\varepsilon_{scat\ 300}$ drastically increased after the incubation period of 5 d like

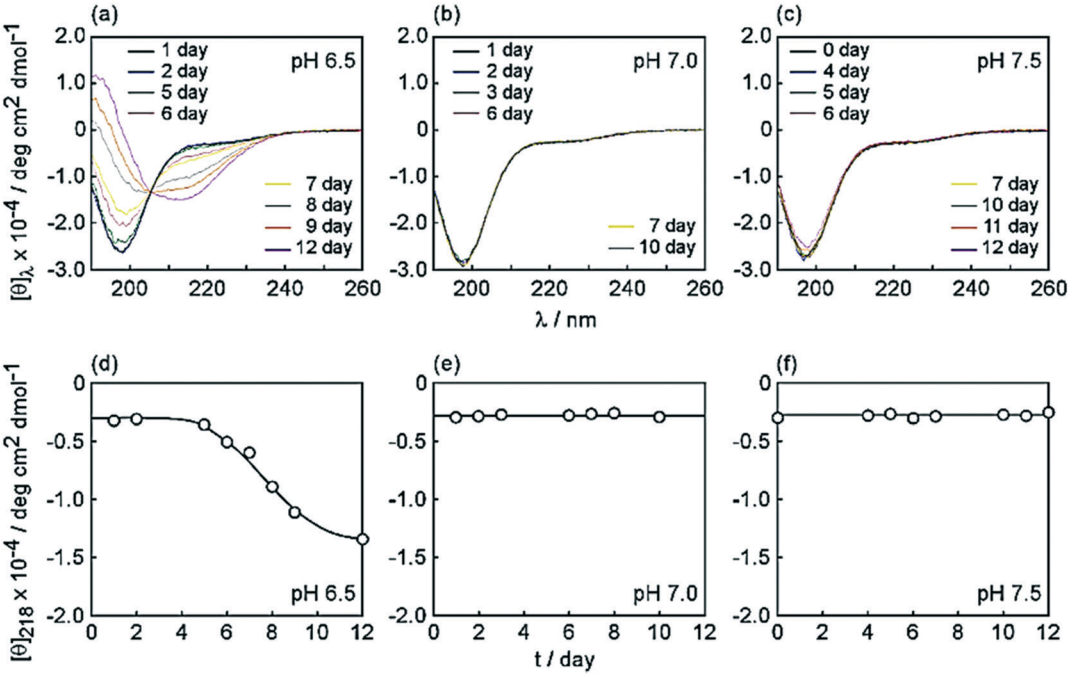

Fig. 1 CD spectra (a–c) and time-dependent changes in molar ellipticity at 218 nm (d–f) for the self-assembly composed of the nucleopeptide and spacer peptide under the various pH conditions, (a and d) pH 6.5, (b and e) pH 7.0, and (c and f) pH 7.5, respectively. The molar ratio of the nucleopeptide and spacer-peptide was fixed at 1 : 5.

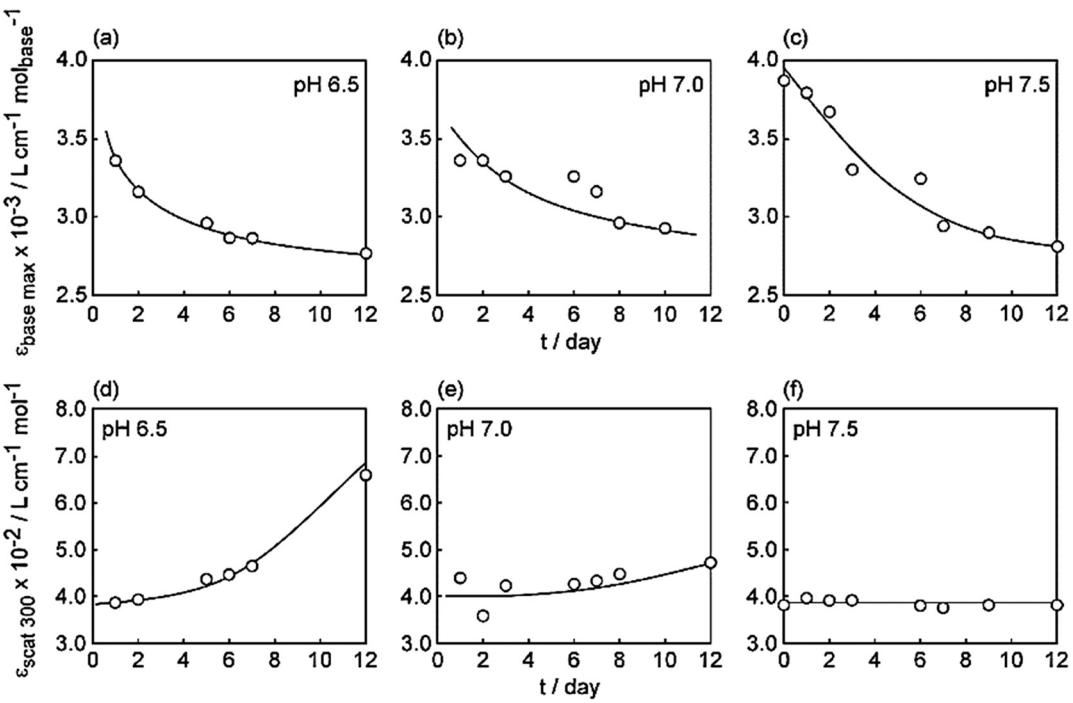

Fig. 2 Time-dependent changes in molar extinction coefficient maxima based on the base pairing around 260 nm (a–c) and the changes in the molar extinction coefficient based on scattering at 300 nm (d–f) for the nucleopeptide/spacer peptide self-assembly under the various pH conditions, (a and d) pH 6.5, (b and e) pH 7.0, and (c and f) pH 7.5, respectively. The molar ratio of the nucleopeptide and spacer-peptide was fixed at 1 : 5.

the conformational transition of the peptide chains (Fig. 1(d)). Only at pH 6.5 were ellipsoid-like assemblies of the sheet structures observed in the aqueous solution after the induction period (Fig. S7†). From these results, the mechanism of the structural changes of the assemblies composed of the nucleopeptide and spacer peptide in the aqueous

solution is explained as follows. The assemblies observed at pH 6.5 were formed with a process of two types of self-organization: base pairing between the nucleotide graft-chains for the early stage of the induction period and β-sheet formation by intermolecular hydrogen bonding between the peptide chains after the induction period. Formation of the base pair would be induced by an increase of the local concentration of the nucleopeptide. An increase of the local concentration is accelerated during β-sheet formation by intermolecular hydrogen bonding between the nucleopeptides and/or spacer peptides. Therefore, it is thought that the induction period for the base pairing was necessary for the conformational transition from a random coil to a β-sheet of the peptide chain. Note that the formation of a β-sheet structure occurred only at pH 6.5, where the degree of protonation of carboxyl groups of Glu side-chains was relatively low. Under relatively low electrostatic repulsion conditions, the nucleopeptides and spacer peptides formed an assembly. The assemblies formed by concerted interactions increased the turbidity of the solution after the induction period. On the other hand, formations of a β-sheet structure were inhibited under pH 7.0 and 7.5 conditions, where the degrees of protonation of carboxyl groups of Glu side-chains were relatively high. Under these pH conditions, the nucleopeptides will be dissolved as dimers that formed only base pairing between the nucleotide graft-chains, and the spacer peptides that existed as monomers took random coil conformations owing to the relatively high electrostatic repulsions.

Fabrication of the self-organized assembly having a nanospace in the interior on the substrates

Kinoshita *et al.* have reported the fabrication of highly aligned two-dimensional (2D) nanosheets consisting of amphiphilic β-sheet peptides on the substrates using the adsorption method.[30] The ordered nanosheets could be obtained by immersing the substrates into a random coil peptide solution. We attempted the formation of a self-organized assembly composed of the nucleopeptides and spacer peptides on the substrates using the adsorption method. Fig. 3 shows the TEM images of the assemblies formed on elastic carbon-coated STEM grids. The assemblies were formed on the STEM grids by immersing the grids into an aqueous solution containing the nucleopeptide and spacer peptide at all the various pH conditions for 10 d at 15 °C. The molar ratio of the nucleopeptide and spacer peptide was fixed at 1 : 5. At pH 6.5, we observed many ellipsoid-like bodies (Fig. 3(a)) that had similar morphologies to those observed in the aqueous system (Fig. S7†), with stacked sheet assemblies (Fig. 3(b)). The observed ellipsoid-like bodies on the substrate were the assemblies that formed in bulk solution. We believe that the ellipsoid-like assemblies were formed by the random intermolecular hydrogen bonding between the β-sheet peptide chains in the bulk. On the other hand, at pH 7.0 (Fig. 3(c)) and 7.5 (Fig. 3(d)), the formation of the ellipsoid-like assemblies was inhibited, and we observed stacked sheets, which were larger than those obtained at pH 6.5.

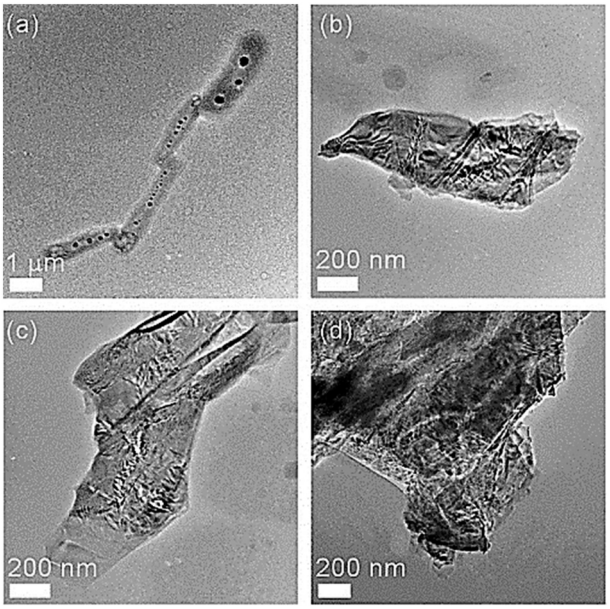

Fig. 3 TEM images of the nucleopeptide/spacer peptide assemblies formed on STEM grids under the various pH conditions, (a and b) pH 6.5, (c) pH 7.0, and (d) pH 7.5 after 10 days of incubation at 15 °C, respectively. The molar ratio of the nucleopeptide and spacer peptide was fixed at 1 : 5.

We investigated the nanostructure in the nanosheets obtained at pH 7.0 and 7.5 conditions by the adsorption method. Under these conditions, the peptide chains took a random coil conformation in the adsorption solutions. Nanolines with 6.0 nm widths were clearly observed in the sheets obtained at pH 7.0 (Fig. 4(a)) and pH 7.5 (Fig. 4(b)). The width of the nanoline, 6.0 nm, corresponded to the molecular length, 5.8 nm, of the peptide main-chain of the nucleopeptide and spacer peptide, which took a β-sheet conformation. The SAED patterns of the nanosheets showed different oriented high order diffraction spots, which corresponded to the distance between the β-strands, 0.47 nm (Fig. 4 insets). Furthermore, we analyzed domains in the peptide sheet by dark field TEM observation based on each SAED spot (Fig. S8†). From the analytical results, we show that each SAED spot is attributed to different domains in the peptide sheet. These results indicate that the nucleopeptide and spacer peptide formed ordered self-organized nanosheets with a conformational transition (from a random coil to β-sheet conformation) on the substrates. That is to say, the adsorbed peptide and nucleopeptide took a β-sheet conformation on the substrate, acting as the nucleus for the growth of the ordered nanosheet by intermolecular hydrogen bonding. The nanostructural analysis by TEM observation suggested that highly aligned β-sheets having different growth directions were stacked to form nucleopeptide/spacer peptide nanosheets. Moreover, we measured the layer thickness of the nucleopeptide/spacer peptide nanosheet by AFM observation (Fig. S9†). From the section analysis profile

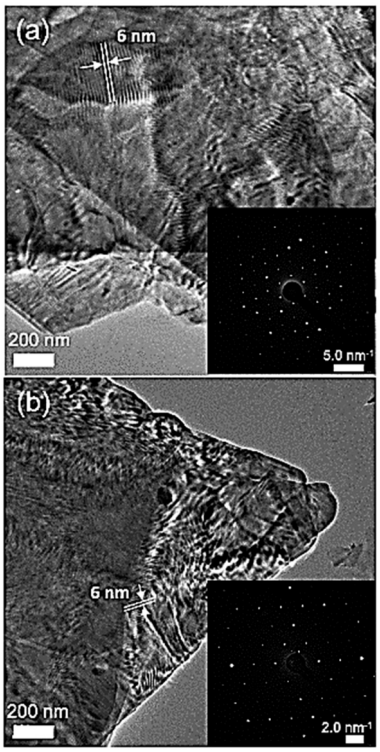

Fig. 4 TEM images and SAED patterns (insets) of the ordered nucleopeptide/spacer peptide nanosheets formed on STEM grids after 10 days of incubation at 15 °C under (a) pH 7.0 and (b) pH 7.5, respectively. The molar ratio of the nucleopeptide and spacer peptide was fixed at 1 : 5.

based on AFM observation, the layer thickness was approximately 3.0 nm. This value is the sum of thicknesses of the nanospace and the outer layers composed of two β-sheets. The thickness of two outer β-sheets corresponds to the intersheet spacing of the cross-β structure, which has been reported to be 1.06 nm.[29] From these, we calculated the thickness of the nanospace to be approximately 1.9 nm. This layer thickness of the nanosheet agreed well with that of the molecular length of the Z-type double helix composed of 3′-(GC)-5s, 2.2 nm.

To optimize the formation of the nanosheet, we studied the relationship between the molar ratio of the nucleopeptide to spacer peptide and the morphology of the nanosheet. We employed another molar ratio of the nucleopeptide to spacer peptide, which was 1 : 6, as a condition for the self-organizational process for nanosheet formation. Fig. 5 shows a TEM image of the nucleopeptide/spacer peptide nanosheet formed on the STEM grid at the molar ratio of 1 : 6. We fixed the other conditions. The STEM grid was immersed into the nucleopeptide/spacer peptide aqueous solution at pH 7.5 for 10 d at 15 °C. A stacked sheet assembly composed of bridged highly arranged β-sheets was observed. The nanostructure of the nanosheet was similar to that of the nanosheet formed at the molar ratio of 1 : 5. Nanolines, whose width was 6.0 nm, were observed in the nanosheet, and the SAED pattern shows different oriented high order diffraction spots (Fig. 5 inset).

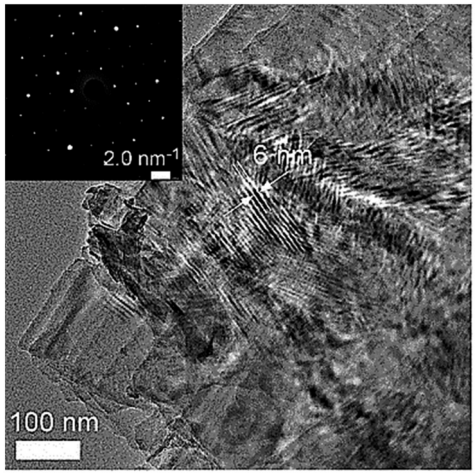

Fig. 5 TEM image and SAED pattern (inset) of the nucleopeptide/spacer peptide nanosheet formed on the STEM grid after 10 days of incubation under pH 7.5. The molar ratio of the nucleopeptide and spacer peptide was fixed at 1 : 6.

However, the size of the nanosheet was larger than that of the nanosheet formed at the molar ratio of 1 : 5. We evaluated the influence of the molar ratio of the nucleopeptide and spacer peptide on the formation of the nanosheet from the areas of the obtained nanosheets, calculated using TEM images. Fig. 6 shows the area distributions of the nanosheets composed of the nucleopeptide and spacer peptide whose molar ratios were 1 : 5 (Fig. 6(a)) and 1 : 6 (Fig. 6(b)). The mean areas of the nucleopeptide/spacer peptide nanosheets formed at molar ratios of 1 : 5 and 1 : 6 were 1.37 μm^2 (coefficient of variation, CV; 1.11) and 13.3 μm^2 (CV; 1.00), respectively. Although the distribution was very wide, the nanosheet formed at the molar ratio of 1 : 6 was 10 times larger than that formed at the molar ratio of 1 : 5. The increase in the area of the nanosheet composed of the nucleopeptide and spacer peptide whose molar ratio was 1.6 is considered as follows. The nucleotide graft-chains of the nucleopeptides are arranged on only one side of the nanoline formed by antiparallel β-sheet peptides at the molar ratio of 1 : 5, when we assume that there is an ideal mixture of the nucleopeptide and

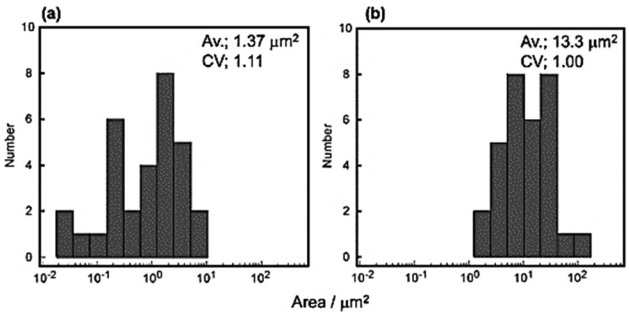

Fig. 6 Histograms for the area of the nanosheets composed of the nucleopeptide and spacer peptide formed on STEM grids after 10 days of incubation under pH 7.5. The molar ratio of the nucleopeptide and spacer peptide was fixed at (a) 1 : 5 and (b) 1 : 6, respectively.

spacer peptide (Fig. S5(a) left†). In this case, the stacking of nanolines induced by the base pairing between the nucleotide graft-chains can form parallel and/or shifted assemblies (Fig. S5(b)†). The specific interactions do not lead to the growth of the nanosheet induced by the side-by-side assembly of these stacked nanolines. On the other hand, the nucleotide graft-chains are arranged alternately on both sides of the nanoline formed at the molar ratio of 1 : 6 (Fig. S5(a) right†). The shifted nanoline nanosheet formed by base pairing has free nucleotide graft-chains. Base pairing of the free nucleotide graft-chains induces the formation of a side-by-side nanosheet of the stacked nanolines. This side-by-side nanosheet of the shifted nanolines formed at the molar ratio of 1 : 6 seems to grow into larger and hierarchical structures (Fig. S5(c)†).

Fabrication of magnetic nano-tape in the nanospace by ferric oxide mineralization

We formed an ordered stacked sheet assembly having a nanospace in the interior *via* a self-organizational process by controlling the pH and molar ratio of the nucleopeptide and spacer peptide. The nanospace faces the carboxylic acids of Glu side-chains at the β-sheet peptides. The carboxylic acids on the template can act as nucleation sites for ferric oxide. We investigated the ferric oxide mineralized in the internal nanospace of the nanosheet. We used the nanospace of the formed nucleopeptide/spacer peptide nanosheet whose molar ratio was 1 : 6 at pH 7.5 as a mineralization template, because a larger and hierarchical nanosheet was obtained at this condition.

Mineralization of ferric oxide was carried out by immersing the substrates immobilizing the nanosheet into an aqueous solution containing a 1 : 2 molar ratio of Fe(II) : Fe(III) at 15 °C for 7 d. EDX elemental mapping (Fig. S10†) showed the formation of the ferric oxide–nucleopeptide/spacer peptide hybrid nanosheet by mineralization from the presence of Fe element based on ferric oxide with N and P elements of the template. From TEM observations (Fig. 7(a)), the morphology of the obtained ferric oxide–nucleopeptide/spacer peptide hybrid maintained the stacked sheet structure from before the mineralization. In the high resolution TEM (HR-TEM) image (Fig. 7(b)), lattice fringes whose distance was 0.3 nm were clearly observed. We determined the crystal phase of the mineralized ferric oxide by SAED pattern analysis (Fig. 7(b) inset). The SAED pattern of the mineralized ferric oxide shows diffraction spots that corresponded to magnetite spacing d_{400} = 2.10 Å and d_{440} = 1.48 Å.[31] In addition, the lattice fringes of 0.3 nm in the HR-TEM image are attributed to the Fe–Fe distance (2.97 Å) in the magnetite d_{100}. The distance between the α-carbons of Glu at the β-sheet peptide was 6.4 Å. This distance was slightly longer than Fe–Fe–Fe distances, 5.94 Å. However, assuming that there was free rotation of the α-carbon–β-carbon bond of Glu, carboxylic acids of the Glu side-chains (movable range; 2.9 Å) at the β-sheet peptides could be in contact with every other Fe atom on the magnetite (1,0,0). Moreover, we calculated the thickness of magnetic nano-tape formable at the nanospace (Scheme 1). We showed that the thickness of the nanospace was 1.9 nm from the AFM result (Fig. S9†). The mineralized magnetite nano-tape in the nanospace would have a thickness of less than two crystal lattices because the length of the *c*-axis of the single crystal lattice of magnetite is 0.84 nm. In fact, we observed many Fe atoms by HR-TEM. This result supports that the mineralized magnetite has a very small thickness. These results indicate that the nanospace sandwiched between β-sheets having Glu side-chains acted as an effective template for magnetite.

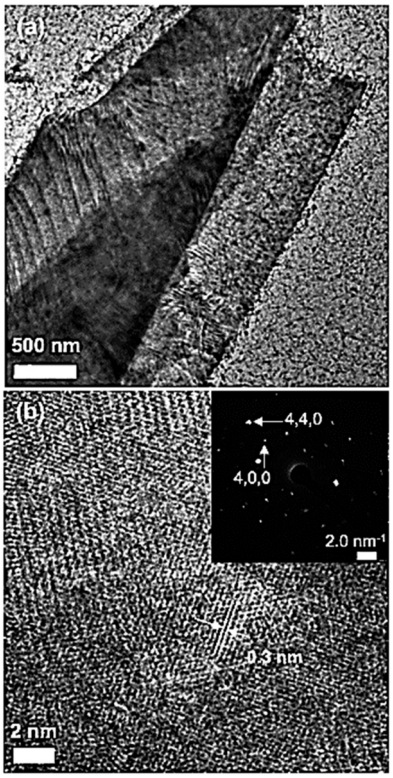

Fig. 7 (a) TEM and (b) HR-TEM images of the nucleopeptide/spacer peptide hybrid nanosheet after mineralization in the nanosheet. The nanosheet formed on the STEM grid after 10 days of incubation under pH 7.5. The molar ratio of the nucleopeptide and spacer peptide was fixed at 1 : 6. Mineralization was carried out for 7 days at 15 °C.

We observed the morphologies of the nanosheet and hybrid nanosheet before/after magnetite mineralization by TEM. As a result, the hierarchical structure of the nanosheets was maintained. For further property analysis, we carried out AFM observation to show not only adhesion contrast but also modulus contrast at parts of the uniform nanosheet surface of the obtained magnetite–nucleopeptide/spacer peptide hybrid nanosheet. The magnetic properties of the hybrid nanosheet were evaluated from the adhesion between the hybrid nanosheets and the magnetized AFM probe by PF-QNM observation. We simultaneously acquired the modulus and height images. Fig. 8 shows the height, modulus, and adhesion images of the nucleopeptide/spacer peptide nanosheet

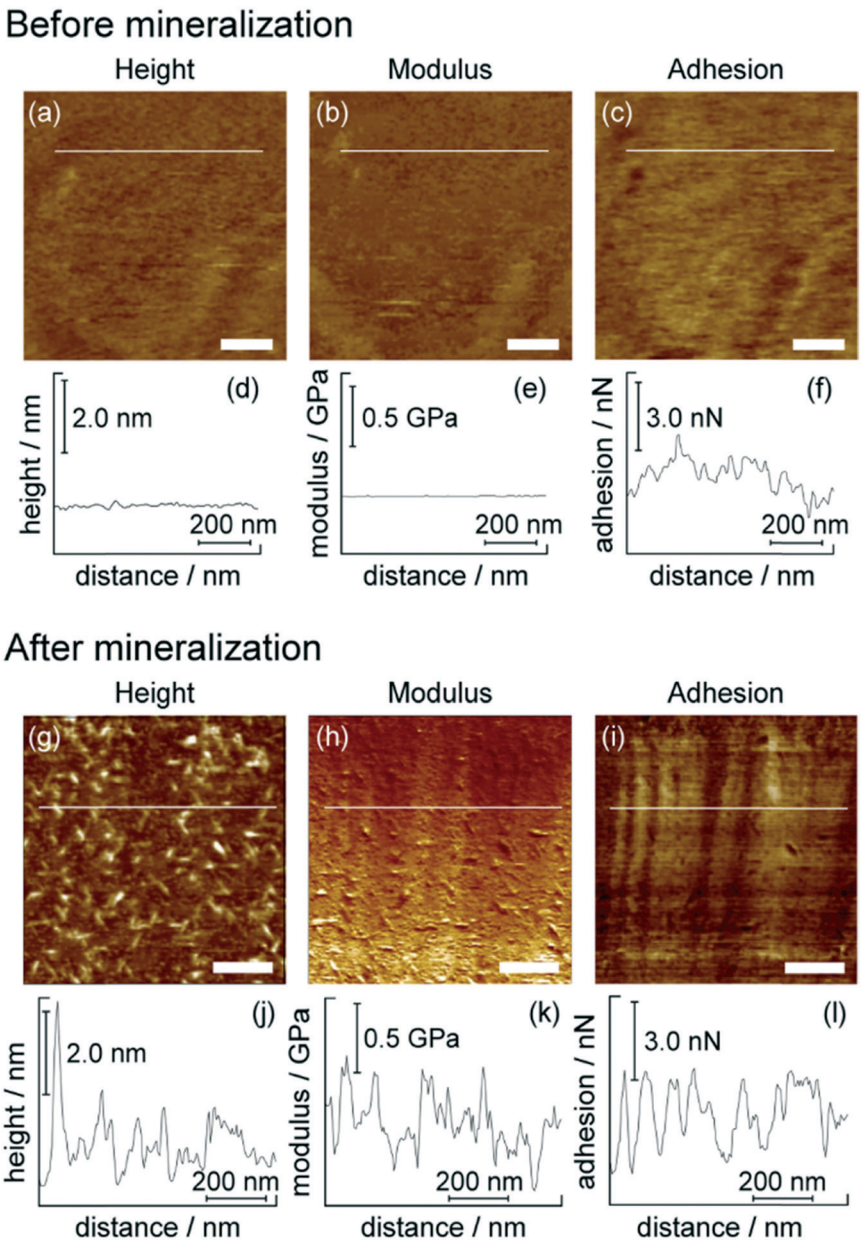

Fig. 8 PF-QNM AFM images of the nucleopeptide/spacer peptide nanosheets (or hybrid nanosheets) before and after mineralization: (a and g) height, (b and h) modulus, and (c and i) adhesion images, respectively. Section analysis profile in white lines in each image shows: (d and j) height, (e and k) modulus, and (f and l) adhesion images, respectively. The molar ratio of the nucleopeptide and spacer peptide was fixed at 1 : 6. The nanosheets formed on the mica after 10 days of incubation under pH 7.5 at 15 °C. Mineralization was carried out for 7 days at 15 °C. Scale bars in the images are 200 nm.

and the magnetite–nucleopeptide/spacer peptide hybrid nanosheet. The section analysis profiles in the white lines of the images are shown in this figure. We used the mica as a substrate for the immobilization of the nucleopeptide/spacer peptide nanosheet. Before mineralization, the height, modulus, and adhesion images of the nucleopeptide/spacer peptide nanosheet were uniform. The mica surface has a slightly negative charge in comparison with the carbon coated STEM grid surface. We could not find clear differences in the morphology of the nanosheets formed on the substrates (STEM grid; Fig. 5, and mica; S9† and 8(a)). This result indicates that the driving force of the immobilization of the nucleopeptide/spacer peptide nanosheet on the substrate is the hydrophobic interaction between the Val side chains of the β-sheet peptide and the substrate. After mineralization, in the height image (Fig. 8(g)), many short fillers were observed. However, in the modulus (Fig. 8(h)) and adhesion (Fig. 8(i)) images of the magnetite–nucleopeptide/spacer peptide hybrid nanosheet, we did not observe short fillers. The fillers were observed in the TEM image (Fig. 7(a)). We believe that the fillers were the adsorbed salts. Furthermore, the modulus and adhesion images after mineralization show clearly different images

compared to those of the nanosheet before mineralization. The modulus and adhesion images of the magnetite–nucleopeptide/spacer peptide hybrid nanosheet show a nano-tape pattern. This result indicates that the mineralized magnetite formed a high modulus region as a nano-tape pattern in the internal nanospace of the nucleopeptide/spacer peptide nanosheet. This hypothesis is also supported by results of the adhesion image. From the adhesion image of the magnetite–nucleopeptide/spacer peptide hybrid nanosheet, a lower adhesion region appeared in the higher modulus region (Fig. 8(i) and (h), and S11†). We used a south pole induced cantilever on the tip surface. This implies that the magnetite nano-tape pattern in the hybrid nanosheet had a magnetic repulsive force. We found an interesting phenomenon in the adhesion image of the magnetite–nucleopeptide/spacer peptide hybrid nanosheet. The mineralized magnetite in the hybrid nanosheet formed an oriented magnetic nano-tape. In other words, a crystal of the mineralized magnetite was oriented by specific mineralization in the internal nanospace of the nucleopeptide/spacer peptide nanosheet. This crystal orientation induced the arrangement of the magnetism in the nanospace.

Conclusions

We investigated the formation mechanisms of the ordered hierarchical nucleopeptide/spacer peptide nanosheet having a nanospace in the interior by a self-organization process. We attempted to fabricate a magnetic nano-tape in the nanospace of the self-organized nanosheet utilizing mineralization. The nucleopeptide/spacer peptide nanosheet was achieved by two types of self-organizational process: (1) formation of a double-helical structure by complementary base paring of the nucleotide graft-chains of the nucleotides in the initial state and (2) formation of highly aligned 2D-nanosheets by adsorption of the peptide chains on substrates with a conformational transition from a random coil to β-sheet structure. The pH condition affected the protonation or deprotonation of the carboxyl group of the Glu side-chain in the nucleopeptide and spacer peptide in the solution. Partial protonation of the carboxyl group at low pH induced the formation of the β-sheet of the peptide chain and aggregate in the solution. As a result, these inhibited the formation of the ordered hierarchical assembly by the self-organization process between the nucleopeptide and spacer peptide on the substrate. The double-helices were formed by the nucleotide graft-chains acting as bridges between the highly aligned 2D nanosheets. The nucleopeptide/spacer peptide nanosheet forms an ordered hierarchical structure with a nanospace in the interior sandwiched by two sheets bridged by nucleotide graft-chains. The structure of the self-organized nanosheets can be controlled by pH and the molar ratio of the nucleopeptide and spacer peptide. Through mineralization in the internal nanospace of the self-organized nanosheet, a magnetic nano-tape was obtained whose crystal orientation and magnetism were controlled. Based on the results of this study, we clarified that the internal nanospace of the self-organized nanosheet as a reaction field is useful for controlling the morphology and crystal structure of the mineralized magnetite. This knowledge of the 3D control of the crystal structure of magnetite is expected to trigger innovations in the field of nanotechnology, including the development of functional nanodevices and self-organizational nanomaterials by bioinspired processes.

Conflicts of interest

There are no conflicts to declare.

References

1 A. Gopinath, E. Miyazono, A. Faraon and P. W. K. Rothemund, *Nature*, 2016, **535**, 401.
2 G. Tikhomirov, P. Petersen and L. Qian, *Nature*, 2017, **552**, 67.
3 A. A. Rafat, T. Prizer, M. Scheible, A. Kostina and F. C. Simmel, *Angew. Chem., Int. Ed.*, 2014, **53**, 7665.
4 F. Zhang, S. Jiang, L. W. Ashley, Y. Liu and H. Yan, *Angew. Chem., Int. Ed.*, 2016, **55**, 8860.
5 Q. Li, Y. Jia, L. Dai, Y. Yang and J. Li, *ACS Nano*, 2015, **9**, 2689.
6 T. Koga, M. Higuchi, T. Kinoshita and N. Higashi, *Chem. – Eur. J.*, 2006, **12**, 1360.
7 C. Zhang, X. Xue, Q. Luo, Y. Li, K. Yang, X. Zhuang, Y. Jiang, J. Zhang, J. Liu, G. Zou and J. X. Liang, *ACS Nano*, 2014, **11**, 11715.
8 K. Murai, T. Kinoshita, K. Nagata and M. Higuchi, *Langmuir*, 2016, **32**, 9351.
9 A. Aggeli, M. Bell, N. Boden, J. E. Kenn, P. F. Knowles, T. C. B. McLeish, M. Pitkeathly and S. E. Radford, *Nature*, 1997, **386**, 259.
10 A. Aggeli, M. Bell, L. M. Carrick, C. W. G. Fishwick, R. Harding, P. J. Mawer, S. E. Radford, S. E. Strong and N. Boden, *J. Am. Chem. Soc.*, 2003, **125**, 9619.
11 G. W. Vandermeulen, C. Tziatzios and H. A. Klok, *Macromolecules*, 2003, **36**, 4107.
12 J. D. Hartgerink, E. Beniash and S. I. Stupp, *Science*, 2001, **294**, 1684.
13 N. Vidavsky, S. Addadi, J. Mahamid, E. Shimoni, D. Ben-Ezra, M. Shpigel, S. Weiner and L. Addadi, *Proc. Natl. Acad. Sci. U. S. A.*, 2014, **111**, 39.
14 S. Blank, M. Arnoldi, S. Khoshnavaz, L. Treccani, M. Kuntz, K. Mann, G. Grathwohl and M. Fritz, *J. Microsc.*, 2003, **212**, 280.
15 M. Kikuchi, S. Itoh, S. Ichinose, K. Shinomiya and J. Tanaka, *Biomaterials*, 2001, **22**, 1705.
16 M. Sumper and N. Kröger, *J. Mater. Chem.*, 2004, **14**, 2059.
17 E. D. Sone and S. I. Stupp, *Chem. Mater.*, 2011, **23**, 2005.
18 K. Murai, M. Higuchi, T. Kinoshita, K. Nagata and K. Kato, *Chem. Commun.*, 2013, **49**, 9947.
19 K. Murai, M. Higuchi, T. Kuno and K. Kato, *ChemPlusChem*, 2014, **79**, 531.

20 K. Murai, Y. Yamamoto, T. Kinoshita, K. Nagata and M. Higuchi, *J. Mater. Chem. B*, 2017, **5**, 5539.
21 K. Murai, K. Kurumisawa, Y. Nomura and M. Matsumoto, *ChemMedChem*, 2017, **12**, 1595.
22 T. Nonoyama, T. Kinoshita, M. Higuchi, K. Nagata, M. Tanaka and K. Kato, *J. Am. Chem. Soc.*, 2012, **134**, 8841.
23 T. Nonoyama, T. Kinoshita, M. Higuchi, K. Nagata, M. Tanaka, K. Sato and K. Kato, *Langmuir*, 2011, **27**, 7077.
24 J. Baumgartner, M. A. Carillo, K. M. Eckes, P. Werner and D. Faivre, *Langmuir*, 2014, **30**, 2129.
25 J. J. M. Lenders, L. A. Bawazer, D. C. Green, H. R. Zope, P. H. H. Bomans, G. With, A. Kros, F. C. Meldrum and N. A. J. M. Sommerdijk, *Adv. Funct. Mater.*, 2017, **27**, 1604863.
26 D. Faivre and T. U. Godec, *Angew. Chem., Int. Ed.*, 2015, **54**, 4728.
27 J. J. M. Lenders, C. L. Altan, P. H. H. Bomans, A. Arakaki, S. Bucak, G. With and N. A. J. M. Sommerdijk, *Cryst. Growth Des.*, 2014, **14**, 5561.
28 J. C. Sutherland, K. P. Griffin, P. C. Keck and P. Takacs, *Proc. Natl. Acad. Sci. U. S. A.*, 1981, **78**, 4801.
29 D. A. Kirschner, C. Abraham and D. J. Selkoe, *Proc. Natl. Acad. Sci. U. S. A.*, 1986, **83**, 503.
30 T. Nonoyama, M. Tanaka, T. Kinoshita, F. Nagata, K. Sato and K. Kato, *Chem. Commun.*, 2010, **46**, 6983.
31 C. Haavik, S. Stølen, H. Fjellvåg, M. Hanfland and D. Häusermann, *Am. Mineral.*, 2000, **85**, 514.